

ShadowMamba: State-Space Model with Boundary-Region Selective Scan for Shadow Removal

Zhu Xiuji^a, Chow Chee-Onn^{a,*} and Chuah Joon Huang^{a,b}

^aDepartment of Electrical Engineering, Faculty of Engineering, Universiti Malaya, Lembah Pantai, Kuala Lumpur, 50603, Malaysia

^bFaculty of Engineering and Information Technology, Southern University College, Skudai, 81300, Malaysia

ARTICLE INFO

Keywords:

Mamba
Scanning mechanism
Image shadow removal
Shadow boundary

ABSTRACT

Image shadow removal is a common low-level vision challenge. Shadows cause sudden brightness changes in some regions, which can hurt the performance of downstream tasks. Current Transformer-based methods often use internal windows to boost efficiency. However, these windows shrink the effective receptive field and reduce the ability to model long-range dependencies. Recently, Mamba has shown impressive results in computer vision by globally modeling long sequences with linear complexity. But when applied directly to shadow removal, the original Mamba scanning ignores the semantic continuity of shadow boundaries and the coherence within each region. To address this issue, this paper proposes a novel selective scanning method called Boundary-Region Selective Scanning. This method divides the image into shadow, boundary, and non-shadow regions, allowing pixels of the same type to be closer together in the sequence. This enhances semantic correlation and helps the model better capture local detail information. In addition, a simple and effective mask denoising method is introduced, which improves the quality of the dataset and enhances the performance of models guided by shadow masks. Based on these techniques, this paper presents ShadowMamba, the first Mamba-based model for shadow removal. Built on the U-Net architecture, ShadowMamba extracts boundary details in shallow layers through boundary-region selective scanning and captures brightness information in deeper layers via global cross-scanning. Extensive experiments demonstrate that ShadowMamba outperforms existing state-of-the-art methods on the AISTD, ISTD, and SRD datasets, while achieving lower parameter counts and computational complexity. Code is available at: <https://github.com/ZHUJIUJINChris/ShadowMamba>.

1. Introduction

Shadows are cast when objects block light, making it inevitable that they are captured in images during acquisition. The presence of shadows not only causes the image to lose certain information but also affects the accuracy of downstream tasks, such as object detection [67, 6], instance segmentation [30, 25], and image classification [5, 53]. Consequently, effective shadow removal is essential for enhancing image quality and improving the performance of these vision tasks.

Shadow removal is a classic low-level vision problem, yet it differs from other tasks such as image super-resolution [46, 9], low-light image enhancement [59, 2], image de-raining [7], and dehazing [52], which involve processing the entire image. In contrast, shadow removal specifically targets the degraded regions within an image, necessitating dedicated modeling of shadowed areas. This selective focus adds to the complexity of the task, making it particularly challenging.

Traditional shadow removal methods are mainly categorized into illumination transfer methods [24, 65] and shadow region relighting methods [13, 15]. These approaches rely on the physical modeling of shadows and are effective for handling single shadow types. However, they often struggle

in complex background scenarios. In recent years, deep learning progressively replaces traditional techniques, giving rise to numerous shadow removal methods [34, 8, 38, 21, 22, 43, 60] based on CNN and Transformer architectures. These methods model shadow images by leveraging brightness information [70, 12], shadow boundary information [48, 23], or regional characteristics [8, 55, 21], employing deep networks to achieve effective shadow removal.

Currently, Transformer-based shadow removal methods show outstanding performance, mainly due to the self-attention mechanism's ability to flexibly capture pixel relationships across regions, enabling the transfer of illumination information or the reconstruction of brightness in shadowed areas. However, the dot-product operations in self-attention exhibit quadratic complexity, causing computational and memory demands to increase rapidly as the sequence length grows. This imposes significant limitations on ViT-based [11] models such as CRFormer [55] when processing high-resolution shadow images. To address this issue, ShadowFormer [21] and HomoFormer [60] use a local window mechanism [45] to reduce computational complexity. However, this strategy cannot compute self-attention over all tokens at once, which inevitably requires a trade-off between the effective receptive field and computational cost. As a result, it limits the model's ability to capture long-range dependencies in shadow images, leading to suboptimal performance.

Recently, an improved structured state-space sequence model called Mamba [17] was proposed. It models long-sequence relationships with linear complexity, has a global

*Corresponding author

✉ s2121087@siswa.um.edu.my (Z. Xiuji); cochow@um.edu.my (C.

Chee-Onn); jhchuah@um.edu.my (C.J. Huang)

ORCID(s): 0009-0002-1017-2474 (Z. Xiuji); 0000-0001-6044-2650 (C. Chee-Onn); 0000-0001-9058-3497 (C.J. Huang)

receptive field, and introduces a novel form of attention through a selective scanning mechanism, achieving performance comparable to Transformers in most tasks. Since Mamba was initially designed for sequence modeling of one-dimensional (1D) data, it employs 1D causal convolutions to process inputs. In the field of computer vision, it is essential to fully consider the relationships between pixels in the upward, downward, left, and right directions to maintain spatial continuity in the scanning sequence. Therefore, many methods enhance the processing performance of two-dimensional (2D) image data by modifying the scanning paths of the selective scanning mechanism. Vim [68] and VMamba [44] were the first to apply Mamba to the visual domain, introducing bidirectional scanning and horizontal-vertical cross-scanning mechanisms. Based on these foundations, numerous Mamba-based visual models, such as Plain-Mamba [62], Mamba-ND [37], ZigMa [28], and LocalMamba [29], have been proposed, significantly improving image task performance by adjusting scanning sequences and enhancing semantic relevance.

Shadow removal primarily relies on information from non-shadow regions to adjust the brightness of shadowed areas, requiring a large receptive field to capture brightness variations across regions. The existing Mamba selective scanning mechanisms [68, 44] and Mamba-based models for image restoration, such as MambaIR [20] and VMambaIR [51], effectively capture global information but partially overlook the semantic correlation of local information. For shadow removal tasks, capturing local detail features is particularly important, especially when dealing with fine details like shadow boundaries. Improper handling of these details can easily lead to boundary artifacts in the restored images. Therefore, it is necessary to introduce a local information scanning mechanism during the shadow removal process to enhance the model's ability to handle boundary local details.

LocalMamba [29] adopts a window mechanism to enhance the semantic correlation of local pixels and scans all windows sequentially. Although this method improves the model's ability to capture local information to some extent, it does not fully consider the characteristics of shadow images. Sequentially scanning windows ignores shadow boundary information, which can easily disrupt the semantic continuity of pixels at shadow boundaries. In addition, this scanning approach causes pixels within the same region to be separated by pixels from other regions, weakening their internal correlation. As a result, pixels with similar semantics become more distant in the long sequence, thereby reducing the model's understanding of semantic relationships in shadow images.

To address these issues, a novel boundary-region selective scanning mechanism is proposed in this paper. This method introduces an additional mask input to divide the shadow image into multiple windows, following a local scanning strategy [29]. According to a set of predefined rules, these windows are classified into shadow regions, boundary regions, and non-shadow regions, forming a new arrangement to scan the original image sequence in the

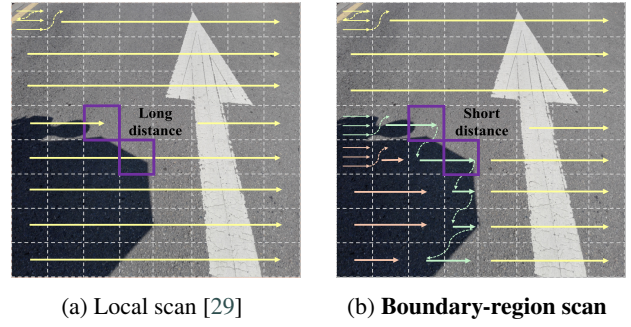


Figure 1: The two purple windows belong to the boundary region of the shadow and exhibit a strong semantic correlation, so their distance in the long sequence should be as close as possible. Regardless of whether the scanning is horizontal or vertical, the proposed boundary-region scanning mechanism effectively reduces their distance in the long sequence. (This is only a rough demonstration, and the actual windows are much smaller.)

updated order. This mechanism enables the separate scanning of the three regions, effectively capturing local details while enhancing the semantic continuity among pixels of the same type. By bringing pixels of the same category closer together in the long sequence, the proposed method improves the model's understanding of local information in shadow images. Figure 1 provides a detailed explanation of the differences between the boundary-region scanning mechanism and the local scanning mechanism.

In addition, this paper also designs a shadow mask denoising method especially for the boundary-region selective scanning mechanism. This method effectively removes noise from non-shadow areas in the mask to ensure the accuracy of the boundary-region selective scanning process. The dataset corrected using this method improves the performance of shadow removal approaches that rely on shadow mask guidance. Finally, based on the boundary-region selective scanning mechanism and the global cross-scanning mechanism, the Boundary Region State-Space Block (BRSSB) and the Global State-Space Block (GSSB) are developed to extract local detail information and global brightness information, respectively. These two modules are integrated through a hierarchical U-Net architecture [50] to build ShadowMamba, the first Mamba-based model specifically designed for shadow removal tasks. The main contributions of this work are summarized as follows:

- This paper is the first to apply the state-space sequence model Mamba to the shadow removal task by designing ShadowMamba, which achieves efficient global token modeling and can handle both hard and soft shadows.
- This paper designs a boundary-region selective scanning mechanism to capture local detail information and improves the semantic continuity among local details in the same region, which helps the model better understand local features.

- This paper proposes a denoising method for shadow masks, which allows the boundary-region selective scanning mechanism to work properly even when the mask contains noise. The dataset corrected using this method helps improve the performance of other models that rely on shadow mask guidance.
- ShadowMamba outperforms existing state-of-the-art (SOTA) methods on standard datasets such as AISTD, ISTD, and SRD, while maintaining lower parameter count and computational complexity.

2. Related work

This section presents related work on image shadow removal, the fundamental concept of Mamba, and its applications in various image restoration tasks.

2.1. Image Shadow Removal

Currently, the work on shadow removal, apart from a few traditional methods based on physical modeling, mainly relies on deep learning approaches, primarily based on CNN and Transformer architectures, with a few models utilizing sequential architectures such as RNN and LSTM.

There are various CNN-based methods for shadow removal. DHAN [10] enhances the receptive field by improving the network structure, achieving better shadow removal results. SP+M+I-Net [34], EMDN [70] and PBID [12] use a linear illumination model, utilizing CNNs to estimate the illumination parameters of shadow regions. AEFNet [14] achieves shadow removal from the perspective of auto exposure fusion. CA-Net [8] and SG-ShadowNet [54] transfer feature information from non-shadow regions to shadow regions, enabling illumination transfer or style transfer for shadow removal. BM-Net [69] uses shadow generation to assist the shadow removal process, guiding it with invariant image information. BA-ShadowNet [48] leverages boundary information for shadow removal, demonstrating the effectiveness of boundary information in shadow removal. Inpaint4shadow [38] models the shadow removal problem as a fusion of image inpainting and shadow removal, achieving excellent performance by fine-tuning the image inpainting network. DMTN [41] effectively improves shadow removal performance through feature decoupling. StructNet [42] guides shadow removal through structural priors.

The attention mechanism of Transformers excels at modeling the relationships between shadow and non-shadow regions, enabling the effective transfer of illumination information. SpA-Former [66] and TSRFormer [3] enhance the receptive field by optimizing the network structure and directly perform shadow removal. CRFormer [55] adopts ViT [11] as its backbone and utilizes a cross-region attention mechanism to compute a correction matrix, which is added to the attention matrix to highlight associated pixels between shadow and non-shadow regions. However, due to the quadratic complexity of ViT, ShadowFormer [21] builds on

Swin-Transformer [45] to limit the computational complexity within the window range. It also employs a cross-region attention mechanism to compute a correction matrix, which is multiplied with the attention matrix to indirectly enable the transfer of information from non-shadow regions to shadow regions. Since ShadowFormer shares weights across windows within the same layer, it is limited in handling non-uniformly degraded soft shadows. To address this issue, HomoFormer [60] adopts a pixel shuffling strategy to homogenize the spatial distribution of shadow degradation and then utilizes a local self-attention mechanism for processing. Additionally, OmniSR [61] integrates semantic features and geometric information, reweighting features within the local attention mechanism to achieve more precise shadow removal. ShadowMaskFormer [39] introduces shadow mask information during the patch embedding stage, enhancing the model's focus on shadow regions.

In addition, generative models based on the aforementioned architectures are emerging, with Diffusion-based [27] shadow removal methods gradually replacing GAN-based [16] approaches. ShadowDiffusion [22] leverages generative and degradation priors to progressively predict more accurate shadow masks, assisting in shadow removal and achieving outstanding results. LFG-Diffusion [47] minimizes the difference between the feature spaces of shadow and shadow-free images to obtain latent features, which contain more useful information than explicit features. DeS3 [32] excels at handling self-shadows by introducing ViT similarity loss, which enables more robust extraction of structural information. RRLSR [43] uses illumination decomposition and a bidirectional correction network to achieve high-quality shadow removal.

2.2. State Space Models

Recently, State-Space Models (SSMs) have gained significant attention in the field of deep learning, emerging as a strong competitor to Transformers. SSM originates from modern control theory and is a model that describes the state representation of sequences at each time step and predicts their next state. Since the original SSM theory deals with continuous functions, Hippo [18] discretizes it and enabled parallelization for training and inference. S4 [19] transforms the Hippo matrix into a normal matrix and a low-rank matrix, improving computational efficiency. Mamba [17] builds on previous work by incorporating a selective scanning mechanism to implement a novel attention mechanism, capable of modeling global information with linear complexity. Through hardware-aware algorithms, it enhances runtime speed and surpasses the performance of Transformers in most tasks.

The emergence of Mamba seems to have broken the monopoly of Transformers, leading to a surge of Mamba-based work across various fields, including natural language processing [56, 40], speech [31, 35], images and videos. The original scanning method of Mamba is designed for 1D data, and when applied to other domains, it overlooks the continuity between adjacent pixels or frames. Therefore,

modifying its scanning method has become a major research focus.

To address the inherent non-causal nature of visual data, Vim [68] proposes bidirectional scanning and incorporates positional information embedding. VMamba [44] introduces a cross-scanning module capable of capturing features in four directions. Plain-Mamba [62] adopts a continuous zigzag scanning pattern, ensuring that each visual token is always adjacent to the previous scanned token. It also incorporates learnable parameters into the B matrix of the state equation to achieve directional awareness. Mamba-ND [37] proposes bidirectional cross-scanning and a multi-head mechanism, emphasizing that the key element for Mamba to adapt to multi-dimensional data is the design of sequence permutations and combinations. LocalMamba [29] performs local scanning within each window and then scans sequentially across all windows, significantly enhancing the model's ability to capture detailed local features. ZigMa diffusion model [28], which is designed within a stochastic interpolant framework, enhances spatial continuity through the zigzag scanning method and optimizes performance by decomposing spatial and temporal sequences. Videomamba [36] and Vivim [63] propose three-dimensional (3D) bidirectional selective scanning and spatiotemporal selective scanning when processing 3D data, enhancing model performance by strengthening the semantic relevance between frames.

2.3. Applications of Mamba in Image Restoration

In the field of image restoration, many tasks have also adopted Mamba architectures and achieved outstanding results. MambaIR [20] introduces local enhancement and channel attention mechanisms to improve Mamba for image restoration. VmambaIR [51] proposes omnidirectional selective scanning, capable of modeling the information flow from different feature dimensions. Pan-Mamba [26] employs a gating mechanism for multi-input feature fusion, focusing on the pansharpening of remote sensing images. Retinexmamba [1] divides the overall architecture into an illumination estimator and a damage restorer for low-light image enhancement. FreqMamba [71] performs local scanning on wavelet packet decomposed frequency band images, employs a cross-scanning mechanism to process the original image, and integrates Fourier transform to handle global input, ultimately producing rain-free images. RainMamba [58] introduces a novel Hilbert scanning mechanism that more accurately captures sequence-level local information in videos, enhancing temporal modeling capabilities. These studies have highlighted Mamba's potential and importance in advancing the field of image restoration.

3. Methodology

This section first introduces the preliminary knowledge of state-space models, and then presents the overall architecture of ShadowMamba. The model adopts a U-Net structure and consists of multiple Region State-Space Blocks (BRSSBs) and Global State-Space Blocks (GSSBs), which

are used to extract local detail information and global brightness features from shadow images, respectively. Next, the design of the boundary-region selective scanning mechanism is explained in detail. Finally, a simple mask denoising method is introduced to better adapt to this scanning mechanism.

3.1. Preliminaries

SSM is a mathematical model used to describe dynamic systems, utilizing state-space variables to represent the internal state of the system. Mathematically, it is typically represented by both the state equation and the output equation:

$$\begin{cases} \dot{h}(t) = Ah(t) + Bx(t) \\ y(t) = Ch(t) + Dx(t) \end{cases} \quad (1)$$

where $\dot{h}(t)$ represents the time derivative of the state vector $h(t)$, which is the state at the next time step, matrices A and B define the relationship between the state $h(t)$ and the input $x(t)$ with the next state $\dot{h}(t)$, while matrices C and D define the relationship between the state $h(t)$ and the input $x(t)$ with the output $y(t)$.

The above process is for continuous functions, and in deep learning applications, it must be discretized. For the input signal, zero-order hold is used [19], and combined with the time scale parameter Δ , the continuous parameters A and B are converted to discrete parameters \bar{A} and \bar{B} , the discrete form is represented as follows:

$$\begin{cases} \dot{h}(t) = \bar{A}h(t) + \bar{B}x(t) \\ y(t) = Ch(t) + Dx(t) \\ \bar{A} = e^{\Delta A} \\ \bar{B} = \Delta A^{-1}(e^{\Delta A} - I) \cdot \Delta B \end{cases} \quad (2)$$

Mamba [17] has a selective scanning mechanism that stands out in the SSM framework. This mechanism can dynamically adjust the B and C matrices based on different inputs, allowing it to automatically select important features. It achieves a novel attention mechanism that maintains linear computational complexity while having a global receptive field.

3.2. Architecture

Similar to most shadow removal models [21, 60], ShadowMamba adopts a U-Net architecture to capture shadow features at different scales. Figure 2 illustrates the overall architecture of ShadowMamba. It is well known that the shallow layers of the U-Net architecture focus on extracting local details of the image, while BRSSB excels at capturing local information and enhances the model's understanding of details through the boundary-region scanning mechanism. Therefore, BRSSB is placed in the first two layers of the U-Net. In the deep layers of the U-Net, as the spatial resolution of the feature maps decreases, the model is more suitable for capturing overall brightness features from a global perspective. Therefore, GSSB is placed in the last two layers of the

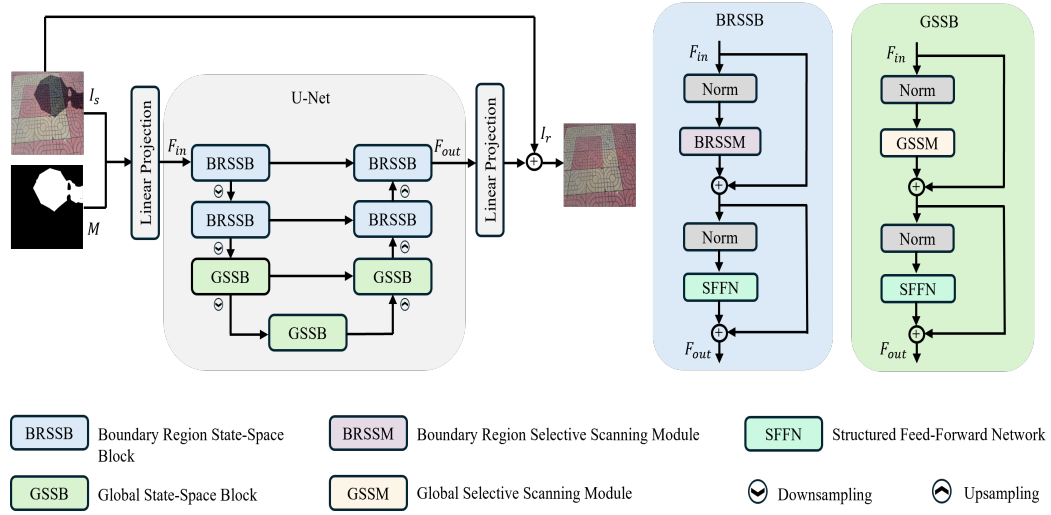


Figure 2: The architecture of the proposed ShadowMamba.

U-Net, utilizing global scanning to restore the brightness of shadow regions.

Specifically, given a shadow input $I_s \in \mathbb{R}^{3 \times H \times W}$ and its corresponding shadow mask $M \in \mathbb{R}^{1 \times H \times W}$, an overlapped embedding is first applied to obtain the shallow feature $F_{in} \in \mathbb{R}^{C \times H \times W}$ from the input. Subsequently, these shallow features are fed into a U-Net architecture composed of multiple BRSSBs and GSSBs, with the decoded output being $F_{out} \in \mathbb{R}^{C \times H \times W}$. Finally, a linear mapping layer is applied to obtain the residual $I_r \in \mathbb{R}^{3 \times H \times W}$ between the output image and the input image.

3.2.1. Boundary Region State-Space Block (BRSSB)

BRSSB follows the classic Transformer architecture design, as shown in the blue section of Figure 2. After the first normalization layer, it integrates the Boundary Region Selective Scanning Module (BRSSM), which incorporates a boundary-region selective scanning mechanism. As the core component of BRSSB, this module effectively captures boundary information and local details within shadow images. After the second normalization layer, the Structured Feed-Forward Network (SFFN) is introduced, primarily to perform structured modeling on the disrupted sequences, enhancing the model's representation capability.

BRSSM: BRSSM integrates the boundary-region selective scanning mechanism, which performs local scans on the feature map from the top, bottom, left, and right directions. This ensures that surrounding local details at any position remain adjacent in the long sequence, thereby enhancing semantic continuity. A detailed introduction to the boundary-region selective scanning mechanism is provided in the next subsection.

In terms of structural configuration, BRSSM is based on the core module VSSB from Vmamba [44], with its detailed structure shown in Figure 3a. The input first passes through a linear embedding layer and is then divided into two information streams. One stream passes through a 3×3

depthwise separable convolution layer and a SiLU activation function before entering the core SSM. The output of the SSM is processed through layer normalization and then fused with the other stream, which is processed only through a SiLU activation function, using the Hadamard product. Finally, the fused information produces the final output.

SFFN: In many Mamba architectures [44, 51], the Feed-Forward Network (FFN) or its variants are commonly used to regulate information flow and enhance the model's expressiveness. ShadowMamba follows a similar design philosophy. However, the proposed boundary-region selective scanning mechanism disrupts the structural order of the original image, leading to limitations in structural information modeling. To address this issue, we directly adopt the structural design from HomoFormer [60], shifting the structure modeling task to the FFN and implementing it as a Structured Feed-Forward Network (SFFN). The detailed architecture is shown in Figure 3c.

Specifically, a deep convolutional layer is inserted between two MLPs, utilizing feature partitioning to enable the CNN to assign weights based on relative positions, thereby achieving structure-based interaction modeling. This design not only enhances the model's feature representation capability but also maintains computational efficiency.

3.2.2. Global State-Space Block (GSSB)

GSSB and BRSSB share the same structural design. The only difference is that BRSSM is replaced by the Global Selective Scanning Module (GSSM), as shown in the green part of Figure 2. The boundary-region selective scanning mechanism in BRSSB is prone to noise interference at low resolutions. This can affect its effectiveness in deeper layers. Additionally, deeper layers in the U-Net structure focus more on high-level semantic information and pay less attention to fine details. To address this, GSSB is applied in the deeper layers of U-Net. It directly captures global brightness

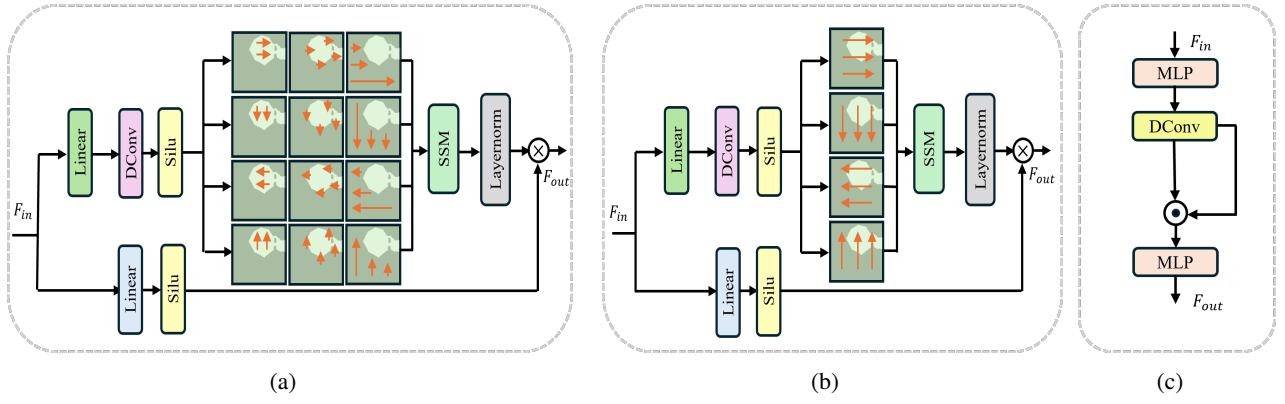


Figure 3: Structural diagrams of each component. (a) Boundary Region Selective Scanning Module (BRSSM). (b) Global Selective Scanning Module (GSSM). (c) Structured Feed-Forward Network (SFFN)

information, helping to restore the brightness of shadowed regions more effectively.

GSSM: The GSSM incorporates a cross-scanning mechanism [44] and follows the same structural design as BRSSM, as shown in Figure 3b. It scans the feature map in four directions: top, bottom, left, and right. This allows each element to gather global information from multiple directions. With this approach, the model can better capture brightness changes from all angles and identify brightness differences between regions.

3.3. Boundary-region selective scanning mechanism

The boundary-region selective scanning mechanism is the core of the method proposed in this paper, specifically designed to cater to image shadow removal. When unfolding a 2D image into a 1D sequence, the arrangement of the sequence is very important, a fact that has been demonstrated in much research. Although Mamba can perform global modeling on long sequences, if semantically related pixels are far apart in a long sequence, it can negatively impact the performance. In other words, the closer semantically related pixels are in a long sequence, the more beneficial it is for modeling in the state-space model.

Shadow boundaries are crucial information in shadow removal, so it is necessary to ensure that the semantics of the pixels at the shadow boundaries remain as continuous as possible, or that their distances in the long sequence are as close as possible. Luminance is the most important factor in shadow removal. In shadow images, the pixels within the shadow region are semantically related due to their similar luminance. In contrast, there is a significant luminance difference between shadow and non-shadow regions, which can be understood as weaker semantic relevance.

Based on the above theory, this paper proposes the boundary-region selective scanning mechanism. It uses windows as the basic unit for sorting. This not only allows the shadow mask to distinguish between shadow and non-shadow regions but also further identifies boundary regions. Based on this, a local scan is performed on the rearranged windows. This approach ensures that pixels of the same type

are closer together in the long sequence, enhancing semantic continuity. At the same time, it improves the model's understanding of local details, especially boundary information, thereby enhancing shadow removal performance. Figure 4 illustrates the working principle of the boundary-region selective scanning mechanism.

Specifically, the input image and its corresponding mask are first divided into windows of the same size. Then, the shadow mask windows are classified according to the following rules:

$$f(W) = \begin{cases} 0, & \text{if } P(W) = \{0\}, \\ 1, & \text{if } P(W) = \{0, 1\}, \\ 2, & \text{if } P(W) = \{1\}. \end{cases} \quad (3)$$

$P(W)$ represents the set of pixel values in window W . When $P(W) = \{0\}$, all pixels in the window are 0, which belongs to category 0, indicating that the window is part of the non-shadow region. When $P(W) = \{0, 1\}$, the window contains both 0 and 1 (255), which belongs to category 1, indicating that the window is part of the boundary region. When $P(W) = \{1\}$, all elements in the window are 1 (255), which belongs to category 2, indicating that the window is part of the shadow region. Figure 4a also illustrates the classification process. Classify all windows and apply this classification information to the shadow image, as shown in Figure 4b. Rearrange the windows according to their categories and sequentially scan the non-shadow region windows, boundary region windows, and shadow region windows, as shown in Figure 4c. This mechanism employs four scanning methods: horizontal, vertical, reverse horizontal, and reverse vertical. The scanning method is the same for both the window interiors and between the windows, allowing for a more comprehensive capture of boundary information in all directions. Figure 4d provides a visual simulation of the scanning sequence. It is evident that windows of the same category are positioned closer together in the long sequence, enhancing the semantic continuity among similar pixels.

The boundary-region selective scanning mechanism differs from the boundary feature modeling approach used

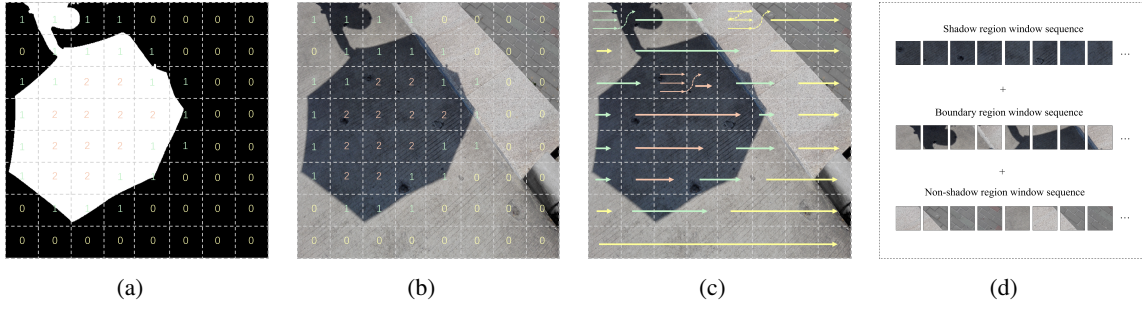


Figure 4: The diagram illustrates the principle of the boundary-region selective scanning mechanism. (a) Uses the shadow mask to divide the windowed regions and determine whether they belong to the shadow area, non-shadow area, or boundary area. (b) After successfully classifying the various windows of the mask, it is applied to the original image. (c) Each category of window is scanned sequentially, performing horizontal and vertical scans respectively. (d) Visualization of the scanning sequence (In the actual model, the window size is 8×8 , this is just a rough demonstration.)

in BA-ShadowNet [48], which processes boundary pixels by separately cropping them. In contrast, the proposed boundary-region selective scanning mechanism does not handle shadow boundaries independently but retains the complete content of both shadow and non-shadow regions, allowing them to be jointly modeled in a long sequence. This not only preserves a certain level of correlation between regions but also enhances the model’s understanding of brightness variations across different regions.

3.4. Mask Denoising Method

Typically, shadow datasets provide clean shadow masks. For datasets without provided masks, shadow detection models [10] are used to generate them. In hard shadow images with clear boundaries, the detected masks are usually accurate and contain little noise, resulting in minimal interference with the boundary-region selective scanning mechanism. However, in soft shadow images with complex backgrounds, the masks often contain holes within the shadow regions or noise points in the non-shadow regions. These issues interfere with the category classification in the boundary-region selective scanning mechanism and negatively affect its modeling performance.

Although common morphological operations such as opening and closing can effectively remove such noise, they often cause shadow boundary shifts. To address the above issue, this paper proposes a simple and effective mask denoising method that focuses on removing noise from the non-shadow regions, as these areas are relatively large and have a greater impact on overall modeling. Although the noise in the shadow regions is not completely removed and may affect the classification between boundary and shadow regions, the method still effectively maintains the semantic continuity between the shadow and non-shadow regions. Specifically, the original mask is sequentially processed using opening and closing operations. The corresponding process is shown in the following formulas:

$$M_{\text{open}} = \text{Dilation}(\text{Erosion}(M)) \quad (4)$$

$$M_{\text{close}} = \text{Erosion}(\text{Dilation}(M_{\text{open}})) \quad (5)$$

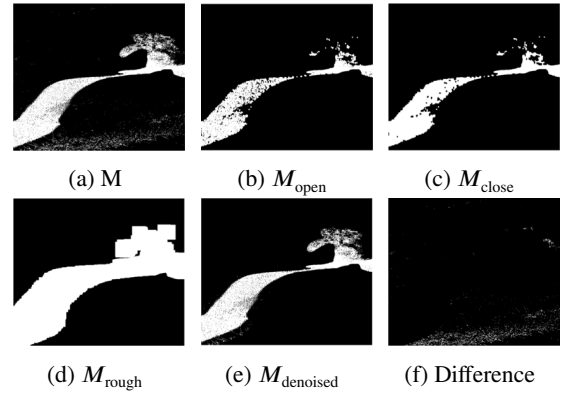


Figure 5: Visualized stages of mask denoising.

Then, a dilation operation is applied to the mask to expand its coverage, resulting in a rough mask. The corresponding formula is shown below:

$$M_{\text{rough}} = \text{Dilation}(M_{\text{close}}) \quad (6)$$

Finally, the original mask is element-wise multiplied with the dilated rough mask to remove noise in the non-shadow regions. The specific formula is as follows:

$$M_{\text{denoised}} = M \cdot M_{\text{rough}} \quad (7)$$

M_{denoised} is the final denoised mask, and Figure 5 illustrates the overall denoising process. This method effectively removes noise in non-shadow regions without altering the shadow boundaries. For models like ShadowFormer [21], which use mask-guided interaction in the deeper layers, this mechanism significantly improves performance. Its effectiveness is further verified in the following ablation studies.

3.5. Loss Function

Only a single Charbonnier loss [4] is used in the proposed method to maintain pixel consistency, as shown in the following formula:

$$L(y, \hat{y}) = \sqrt{(y - \hat{y})^2 + \epsilon^2} \quad (8)$$

where y is the ground truth shadow-free image, \hat{y} is the predicted image output. ϵ is a small constant added to avoid numerical instability.

4. Experiments

4.1. Implementation Details

The proposed ShadowMamba model is implemented using the PyTorch framework, and training is conducted on an RTX 4080 GPU. The network has a channel width of 32, and the batch size is set to 2. In its U-Net structure, the numbers of BRSSB and GSSB modules are [2, 2, 2, 2, 2, 2, 2]. The data augmentation techniques used include horizontal and vertical flipping, as well as Mixup augmentation [64]. The AdamW optimizer is employed to update the learnable parameters, with the initial learning rate set to 2×10^{-4} , gradually decaying to 1×10^{-6} using a cosine annealing strategy.

During the experimental phase, this study adopts three commonly used datasets in the shadow removal domain: ISTD [57], AISTD [33], and SRD [49]. The ISTD dataset primarily contains hard shadows with clear boundaries and includes 1,330 training samples and 540 testing samples. Each sample is a triplet consisting of a shadow image, a mask, and a shadow-free image, with the provided masks containing almost no noise. Due to lighting inconsistencies between the shadow and shadow-free images in ISTD, AISTD applies image processing algorithms to correct this issue and contains the same number of samples as ISTD. The SRD dataset includes both soft and hard shadows, features more complex backgrounds, and consists of 2,680 training samples and 408 testing samples. Each sample is a pair of shadow and shadow-free images, with no masks provided. Following previous studies [21, 47], this study uses the masks predicted by DHAN [10] during training and testing, which contain a relatively high level of noise.

Similar to previous work [34, 12], the Root Mean Absolute Error (RMAE) in the Lab color space is used as an evaluation metric. Additionally, Peak Signal-to-Noise Ratio (PSNR) and Structural Similarity (SSIM) are employed to evaluate image performance in the RGB color space. Note that a lower RMAE indicates better performance, while higher PSNR and SSIM values represent better results. For computational efficiency, FLOPs are measured on 256×256 input images.

4.2. Comparison with State-of-the-Art Methods

The proposed ShadowMamba is compared with the most popular state-of-the-art shadow removal models, including AEFNet [14], CA-Net [8], EMDN [70], SG-ShadowNet [54], BA-ShadowNet [48], BM-Net [69], Inpaint4shadow [38], ShadowFormer [21], ShadowDiffusion [22], DMTN [41], StructNet [42], LFG-Diffusion [47], DeS3 [32], RRLSR [43], HomoFormer [60], OmniSR [61], and ShadowMaskFormer [39]. To guarantee fair comparison, the results of these compared methods are provided by the authors or obtained from the original paper.

4.2.1. Quantitative measure

Table 1, 2&3 show the quantitative results on the testing sets over AISTD, SRD, and ISTD respectively. It can be seen that our method demonstrates performance advantages on both hard shadow and soft shadow datasets.

On the hard shadow datasets AISTD [33] and ISTD [57], the boundary-region selective scanning mechanism fully exploits its advantages due to the provided masks having clear boundaries with minimal noise. ShadowFormer [21] and HomoFormer [60] are limited by local window mechanisms, making it difficult to achieve unified modeling at a global scale. By comparison, ShadowMamba possesses a global receptive field, resulting in superior performance. Moreover, ShadowMamba outperforms diffusion-based methods such as ShadowDiffusion [22], LFG-Diffusion [47], and RRLSR [43]. Although diffusion models have an advantage in generation quality, they are slow in inference. In contrast, ShadowMamba is both fast and highly effective.

On the soft shadow dataset SRD [49], ShadowMamba achieves performance comparable to the SOTA model HomoFormer [60] and significantly outperforms DeS3 [32], which is specifically designed for soft shadow removal. The boundary-region selective scanning mechanism used in ShadowMamba takes windows as basic units, allowing the model to effectively capture local information along wide soft shadow boundaries. In addition, the mask denoising method reduces the impact of large-area noise, enabling good semantic continuity within each region even when the soft shadow masks contain noise.

Table 4 presents a comparison of the models in terms of computational complexity and the number of parameters. ShadowMamba significantly reduces the number of parameters, mainly due to its hierarchical design strategy, where shallow and deep layers take on different roles instead of combining both local and global operations within a single block. This design effectively lowers the overall parameter count. In addition, ShadowMamba also has slightly lower computational complexity than HomoFormer [60], the previously best-performing model based on a window attention mechanism. This further highlights ShadowMamba's efficiency while maintaining strong performance.

4.2.2. Qualitative measure

To further demonstrate the advantages of ShadowMamba over competing methods, visual result comparisons on the AISTD and SRD datasets are shown in Figure 6 and Figure 7. The results show that the proposed method produces fewer boundary artifacts and achieves a more natural balance between the restored shadow areas and the non-shadow areas.

4.3. Ablation Study

To better understand the ShadowMamba method, the boundary-region selective scanning mechanism, and the mask denoising approach, we conduct ablation studies and related analysis on the AISTD dataset [33] and the SRD dataset [49].

Table 1

Quantitative comparisons with the SOTA methods on the AISTD dataset [33].

Size	Method	All Image (ALL)			Shadow Region (S)			Non-Shadow Region (NS)		
		PSNR↑	SSIM↑	RMAE↓	PSNR↑	SSIM↑	RMAE↓	PSNR↑	SSIM↑	RMAE↓
256×256	AEFNet [14]	29.45	0.861	4.23	36.04	0.978	6.55	31.16	0.894	2.40
	BA-ShadowNet [48]	34.60	0.971	3.00	38.29	0.991	5.90	38.48	0.984	3.25
	Inpaint4Shadow [38]	34.16	0.967	3.35	38.10	0.990	6.09	37.66	0.981	2.82
	ShadowDiffusion [22]	<u>35.67</u>	0.975	2.72	<u>39.69</u>	0.992	4.97	38.89	0.987	2.28
	StructNet [42]	34.26	0.969	-	37.92	0.991	-	37.72	0.983	-
	DeS3 [32]	31.38	0.957	3.85	36.49	0.989	6.59	34.72	0.972	3.32
	RRLSR [43]	34.96	0.968	2.87	38.04	0.990	5.69	39.15	0.984	2.31
	HomoFormer [60]	35.35	0.975	<u>2.64</u>	39.49	0.993	4.73	38.75	0.984	<u>2.23</u>
	ShadowMamba	35.74	0.975	2.59	39.96	0.993	<u>4.77</u>	<u>39.05</u>	<u>0.986</u>	2.17
640×480	SG-ShadowNet [54]	30.50	0.930	4.28	35.96	0.984	6.73	32.76	0.950	3.82
	BM-Net [69]	31.85	<u>0.941</u>	3.73	36.80	0.987	6.32	34.47	0.958	3.25
	ShadowFormer [21]	<u>32.78</u>	0.939	<u>3.61</u>	<u>38.07</u>	0.986	6.02	35.14	0.955	<u>3.15</u>
	LFG-Diffusion [47]	32.11	0.936	3.89	37.74	0.987	<u>5.91</u>	34.30	0.951	3.51
	OminiSR [61]	31.35	0.939	3.87	36.16	0.986	7.18	34.41	0.956	3.25
	ShadowMamba	32.85	0.943	3.42	38.43	0.987	5.51	<u>35.09</u>	0.958	3.03

Table 2

Quantitative comparisons with the SOTA methods on the SRD dataset [49].

Size	Method	All Image (ALL)			Shadow Region (S)			Non-Shadow Region (NS)		
		PSNR↑	SSIM↑	RMAE↓	PSNR↑	SSIM↑	RMAE↓	PSNR↑	SSIM↑	RMAE↓
256×256	AEFNet [14]	28.40	0.893	6.50	32.26	0.966	9.55	31.87	0.945	5.74
	EMDN [70]	31.72	0.952	4.79	34.94	0.980	7.44	35.85	0.982	3.74
	BM-Net [69]	31.69	0.956	4.46	35.05	0.981	6.61	36.02	0.982	3.61
	Inpaint4Shadow [38]	33.27	0.967	3.81	36.73	0.985	5.70	36.70	0.985	3.27
	ShadowFormer [21]	32.46	0.957	4.28	35.55	0.982	6.14	36.82	0.983	3.54
	ShadowDiffusion [22]	34.73	0.970	3.63	38.72	<u>0.987</u>	4.98	37.78	0.985	3.44
	DeS3 [32]	34.11	0.968	3.56	37.91	0.986	5.27	37.45	0.984	3.03
	OminiSR [61]	32.87	0.969	-	-	-	-	-	-	-
	HomoFormer [60]	35.37	<u>0.972</u>	<u>3.33</u>	<u>38.81</u>	<u>0.987</u>	4.25	39.45	<u>0.988</u>	<u>2.85</u>
	ShadowMamba	<u>35.32</u>	0.980	3.25	39.07	0.990	<u>4.85</u>	<u>39.25</u>	0.993	2.64

Table 3

Quantitative comparisons with the SOTA methods on the ISTD dataset [57].

Size	Method	All Image (ALL)			Shadow Region (S)			Non-Shadow Region (NS)		
		PSNR↑	SSIM↑	RMAE↓	PSNR↑	SSIM↑	RMAE↓	PSNR↑	SSIM↑	RMAE↓
256×256	CANet [8]	27.39	0.854	5.56	34.90	0.977	7.45	28.70	0.885	5.19
	BM-Net [69]	30.28	0.959	5.02	35.61	0.988	7.34	32.80	0.976	4.57
	EMDN [70]	29.98	0.944	5.22	36.27	0.986	7.78	31.85	0.965	4.72
	StructNet [42]	30.32	0.963	-	36.40	0.989	-	32.27	0.978	-
	DMTN [41]	30.42	0.965	-	35.83	0.990	-	33.01	0.979	-
	ShadowFormer [21]	<u>32.21</u>	<u>0.968</u>	<u>4.09</u>	<u>38.19</u>	0.991	<u>5.96</u>	<u>34.32</u>	0.981	<u>3.72</u>
	ShadowMaskFormer [39]	-	-	4.23	-	-	6.08	-	-	3.86
	ShadowMamba	32.78	0.970	4.06	38.90	0.991	5.83	34.97	0.981	3.71

**Figure 6:** Qualitative results comparing ShadowMamba with other methods on the AISTD dataset (model names abbreviated).

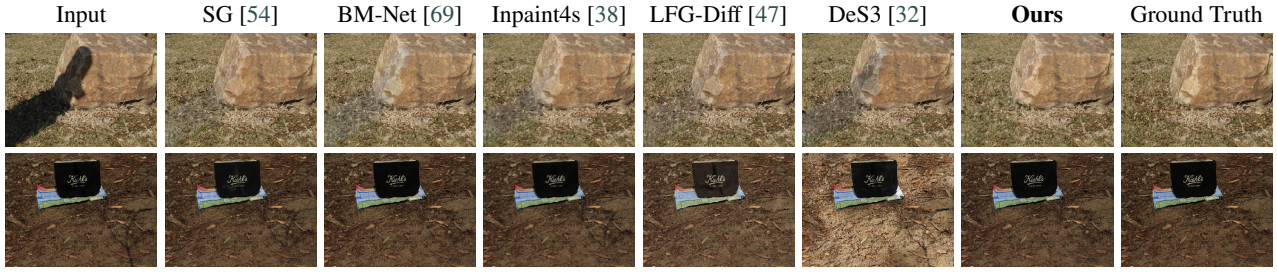


Figure 7: Qualitative results comparing ShadowMamba with other methods on the SRD dataset (model names abbreviated).

Table 4

Quantitative comparison of the methods' computational efficiency in terms of the number of trainable parameters (in million, M) and FLOPs (in billion, G).

Size	Method	Params (M)↓	FLOPs (G)↓
256×256	ShadowDiffusion [22]	60.74	937.15
	Inpaint4Shadow [38]	14.98	81.18
	StructNet [42]	67.06	45.95
	ShadowFormer [21]	11.35	64.60
	HomoFormer [60]	17.81	35.63
	ShadowMamba	6.45	34.71

4.3.1. Effectiveness of hierarchical combination

ShadowMamba adopts a U-Net structure, using BRSSB in the shallow layers to capture local detail features and GSSB in the deeper layers to extract global brightness information. This design captures different types of features while avoiding extra computational cost and redundant information. In addition to the default BRSSB-GSSB combination, this study also explores other block arrangements. Moreover, a dual-branch structure is introduced, which has been applied in several other Mamba models [71, 58]. It combines global and local scanning features within a single block and is referred to as the Dual-Branch State-Space Block (DSSB). The experimental results are shown in Table 5. The results show that the layered combination of BRSSB and GSSB (No.6) achieves the best performance. Compared to the DSSB combination (No.5), this arrangement significantly reduces the number of parameters and computational complexity.

4.3.2. Effectiveness of Each Module

To evaluate the role of each core module in ShadowMamba, this study conducts an ablation experiment on the AISTD dataset, with the results shown in Table 6. The results show that removing any module leads to a drop in performance, and each module is both simple in structure and irreplaceable. This further indicates that BRSSM effectively extracts local details from shadow images, GSSM accurately extracts global brightness variations, and SFFN performs well in modeling the structure of the reordered sequences.

4.3.3. Effectiveness of region-boundary scanning mechanism

To evaluate the effectiveness of different scanning mechanisms in shadow removal, this study replaces the scanning method in the BRSSM module while keeping the overall network structure unchanged. The experimental results are shown in Table 7. Specifically, Design 1 uses global scanning in both shallow and deep layers as the baseline model. Design 2 adopts a region scanning mechanism developed in this study, which divides the image into two regions and scans them sequentially to enhance semantic consistency within each region. Design 3 applies a local scanning method [29] without window rearrangement. Design 4 is the original ShadowMamba model.

The baseline model in Design 1 lacks the ability to model both local details and boundary priors, resulting in the weakest performance. Design 2 maintains semantic continuity within regions but fails to capture local details and does not effectively utilize boundary priors, leading to no performance improvement. Design 3 enhances the perception of local features through local scanning and brings some improvement, but it still struggles with grouping similar pixels and modeling boundary information. In contrast, ShadowMamba's boundary-region selective scanning mechanism not only captures local details but also strengthens semantic connections, leading to a significant improvement in overall performance.

4.3.4. Effectiveness of mask denoising method

This study conducts an ablation experiment on the SRD dataset to evaluate the mask denoising method, as the masks in this dataset contain a large amount of noise. By removing noise from the non-shadow regions of the mask, most interference can be eliminated. The remaining noise in the shadow regions or near the boundaries does not affect the window rearrangement in non-shadow areas. Therefore, even in the presence of some noise, this method can still effectively achieve accurate classification of the two region types and maintain semantic consistency within each region. Table 8 presents the specific performance of the proposed denoising method on the SRD dataset.

Another notable contribution of the proposed denoising method is its ability to improve the accuracy of models that rely on mask-guided region interaction. Taking ShadowFormer [21] as an example, it introduces a mask-based

Table 5

Ablation study for investigating different block arrangements of shadowMamba on the AISTD Dataset. (BR denotes BRSSB, G denotes GSSB, and D denotes DSSB. Each layer contains 2 blocks.)

	Block Arrangement Combinations	ALL PSNR	S PSNR	NS PSNR
1	[G, G, G, G, G, G, G]	35.21	39.73	38.80
2	[BR, G, G, G, G, G, BR]	34.90	39.53	38.64
3	[BR, BR, BR, G, BR, BR, BR]	34.92	39.51	38.66
4	[BR, BR, BR, BR, BR, BR, BR]	35.13	39.66	38.74
5	[D, D, D, D, D, D, D]	35.66	39.90	38.99
6	[BR, BR, G, G, G, BR, BR]	35.74	39.96	39.05

Table 6

Ablation study of different modules of ShadowMamba on the AISTD Dataset.

	Variant Models	ALL PSNR	S PSNR	NS PSNR
1	w/o BRSSM	35.01	39.36	38.53
2	w/o GSSM	34.86	39.31	38.44
3	w/o SFFN	34.48	39.20	38.35
4	ShadowMamba	35.74	39.96	39.05

shadow interaction attention in the deeper layers (L2 and L3) of the U-Net structure. During the upsampling stage, the mask undergoes a MaxPooling operation. While this helps fill small holes within the shadow regions, it also significantly amplifies noise in the non-shadow areas, negatively affecting the model's performance on the SRD dataset. After applying the corrected masks, the model shows a clear performance improvement on SRD. Figure 8 presents a comparison of the upsampling results before and after denoising, showing that the proposed method effectively reduces noise in non-shadow regions, with the effect becoming more noticeable in deeper layers.

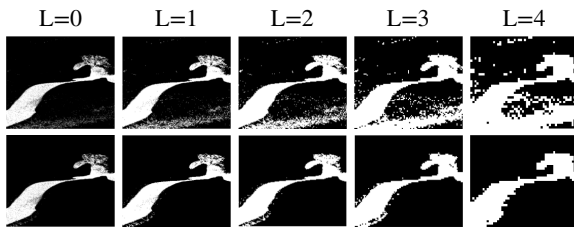


Figure 8: MaxPooling-based upsampling operation on the mask before and after denoising. (The first row shows the results before denoising, and the second row shows the results after denoising. L indicates the number of downsampling layers.)

4.3.5. Impact of window size

The choice of window size is crucial for the boundary-region selective scanning mechanism. Table 9 presents a performance comparison under different window sizes. Experimental results show that when the window size is set to 8 or 10, the model achieves the best balance between accuracy and computational efficiency, resulting in the most optimal

overall performance. During training, randomly cropped 320×320 images are used; in the testing phase, the original image resolution is applied, and the output is finally resized to 256×256 for evaluation.

4.3.6. Impact of mask accuracy

To systematically analyze the impact of mask accuracy on the boundary-region selective scanning mechanism, this study uses the AISTD dataset, which contains nearly noise-free masks, as the basis. Different types and levels of disturbances are artificially injected into the clean masks to simulate various interference scenarios. Three types of disturbances are designed. First, salt-and-pepper noise is added to simulate common random noise. Second, the shadow boundaries are dilated or eroded to reflect inaccurate boundary conditions. Third, large holes are introduced into the masks to simulate certain extreme cases. These types of disturbances together provide a comprehensive evaluation of the mechanism's robustness and fault tolerance. It is worth noting that the correct mask is used for fusion in the initial stage, and noise is injected only during the boundary-region selective scanning process. This setup is intended to specifically highlight the impact of the mask on the boundary-region selective scanning mechanism.

Table 10 shows the impact of mask accuracy on model performance. The results indicate that all three types of disturbances weaken the classification ability of the boundary-region selective scanning mechanism. In the experiments, as the disturbance level increases, the model performance gradually drops and eventually becomes close to that of using local scan in the first two layers. Therefore, it can be inferred that when the mask is accurate, the boundary-region selective scanning mechanism can effectively gather pixels of the same category, enhance semantic continuity, and improve the model's ability to capture local details. However, when the mask classification is inaccurate, the mechanism degrades to a basic local scan, only serving to extract local features.

4.4. Discussion and future work

The boundary-region selective scanning mechanism is designed to shorten the distance between pixels of the same category in long sequences, enhancing their semantic continuity and improving shadow removal performance. ShadowMamba makes full use of the U-Net's hierarchical structure

Table 7

Ablation study of different scanning mechanisms on the AISTD dataset.

	Scanning Mechanism	ALL PSNR	S PSNR	NS PSNR
1	All Global scan	35.21	39.73	38.80
2	Region scan + Global scan	35.23	39.75	38.81
3	Local scan + Global scan	35.46	39.81	38.82
4	Boundary-Region scan + Global scan	35.74	39.96	39.05

Table 8

Ablation study of mask denoising method on the SRD dataset.

	Configuration	ALL PSNR↑	S PSNR↑	NS PSNR↑
1	ShadowFormer [21] w/o mask denoising	32.46	35.55	36.82
2	ShadowFormer w mask denoising	34.13	38.76	38.73
3	ShadowMamba w/o mask denoising	34.96	38.88	38.97
4	ShadowMamba w mask denoising	35.32	39.07	39.25

Table 9

Ablation study of window size on the AISTD dataset.

	Window Size	ALL PSNR	S PSNR	NS PSNR
1	4×4	35.61	39.88	38.92
2	8×8	35.74	39.96	39.05
3	10×10	35.73	39.95	39.07
4	16×16	35.65	39.82	39.03

and designs the shallow and deep layers based on shadow image characteristics. However, this mechanism also has certain limitations. For example, when multiple shadow regions appear in the same image, the boundary-region selective scanning mechanism may fail to work properly. It is worth noting that even in such complex cases, the mechanism still retains the basic function of local scanning.

Another key advantage of ShadowMamba is its ability to model all tokens at once, unlike Transformers that only perform self-attention on a subset of tokens. This feature improves overall performance and enhances the model's potential for complex visual tasks, aligning with future trends in image modeling.

In addition, ShadowMamba has good scalability and can be extended to other mask-based tasks such as image matting and watermark removal, improving the model's ability to perceive and understand local boundary information. In the future, the model will be further developed into a generative shadow removal framework based on Mamba, tailored to the characteristics of shadow images, to further enhance its performance in real-world scenarios.

5. Conclusion

This paper presents a shadow removal model based on the Mamba architecture, called ShadowMamba, which is the first to apply Mamba to this task. The model adopts a hierarchical U-Net structure, where the shallow layers extract local features and the deep layers capture global

brightness information. This design not only enables the extraction of various shadow features but also reduces computational cost. Based on the characteristics of shadow images, a boundary-region selective scanning mechanism is designed to classify and rearrange the divided windows. This enhances the semantic continuity of pixels in similar regions and improves the model's ability to capture local details. In addition, a simple and effective mask denoising method is proposed, which not only improves the accuracy of the boundary-region selective scanning mechanism but also boosts the performance of other mask-guided models. Experimental results show that ShadowMamba outperforms existing methods in both hard and soft shadow scenarios, while also having advantages in parameter count and computational complexity.

References

- [1] Bai, J., Yin, Y., He, Q., 2024. Retinexmamba: Retinex-based mamba for low-light image enhancement. arXiv preprint arXiv:2405.03349.
- [2] Cai, Y., Bian, H., Lin, J., Wang, H., Timofte, R., Zhang, Y., 2023. Retinexformer: One-stage retinex-based transformer for low-light image enhancement, in: Proceedings of the IEEE/CVF International Conference on Computer Vision, pp. 12504–12513.
- [3] Chang, H.E., Hsieh, C.H., Yang, H.H., Chen, I., Chen, Y.C., Chiang, Y.C., Huang, Z.K., Chen, W.T., Kuo, S.Y., et al., 2023. Tsrformer: Transformer based two-stage refinement for single image shadow removal, in: Proceedings of the IEEE/CVF Conference on Computer Vision and Pattern Recognition, pp. 1436–1446.
- [4] Charbonnier, P., Blanc-Feraud, L., Aubert, G., Barlaud, M., 1994. Two deterministic half-quadratic regularization algorithms for computed imaging, in: Proceedings of 1st international conference on image processing, IEEE, pp. 168–172.
- [5] Chen, C.F.R., Fan, Q., Panda, R., 2021a. Crossvit: Cross-attention multi-scale vision transformer for image classification, in: Proceedings of the IEEE/CVF international conference on computer vision, pp. 357–366.
- [6] Chen, S., Sun, P., Song, Y., Luo, P., 2023a. Diffusionidet: Diffusion model for object detection, in: Proceedings of the IEEE/CVF international conference on computer vision, pp. 19830–19843.
- [7] Chen, X., Li, H., Li, M., Pan, J., 2023b. Learning a sparse transformer network for effective image deraining, in: Proceedings of the

Table 10

Impact of Different mask disturbances on model performance (PSNR on AISTD dataset)

	Types of disturbances	Level of disturbance		
		Low	Medium	High
1	Salt-and-pepper noise	35.72	35.58	35.51
2	Inaccurate boundary	35.58	35.53	35.43
3	Hole disturbance	35.73	35.67	38.59
4	ShadowMaba (No disturbance)	35.74	35.74	35.74

- IEEE/CVF Conference on Computer Vision and Pattern Recognition, pp. 5896–5905.
- [8] Chen, Z., Long, C., Zhang, L., Xiao, C., 2021b. Canet: A context-aware network for shadow removal, in: Proceedings of the IEEE/CVF international conference on computer vision, pp. 4743–4752.
- [9] Chu, X., Chen, L., Yu, W., 2022. Nafssr: Stereo image super-resolution using nafnet, in: Proceedings of the IEEE/CVF conference on computer vision and pattern recognition, pp. 1239–1248.
- [10] Cun, X., Pun, C.M., Shi, C., 2020. Towards ghost-free shadow removal via dual hierarchical aggregation network and shadow matting gan, in: Proceedings of the AAAI Conference on Artificial Intelligence, pp. 10680–10687.
- [11] Dosovitskiy, A., 2020. An image is worth 16x16 words: Transformers for image recognition at scale. arXiv preprint arXiv:2010.11929 .
- [12] Einy, T., Immer, E., Vered, G., Avidan, S., 2022. Physics based image deshadowing using local linear model, in: Proceedings of the IEEE/CVF conference on computer vision and pattern recognition, pp. 3012–3020.
- [13] Finlayson, G.D., Drew, M.S., Lu, C., 2009. Entropy minimization for shadow removal. International Journal of Computer Vision 85, 35–57.
- [14] Fu, L., Zhou, C., Guo, Q., Juefei-Xu, F., Yu, H., Feng, W., Liu, Y., Wang, S., 2021. Auto-exposure fusion for single-image shadow removal, in: Proceedings of the IEEE/CVF conference on computer vision and pattern recognition, pp. 10571–10580.
- [15] Gong, H., Cosker, D., 2014. Interactive shadow removal and ground truth for variable scene categories, in: BMVC 2014-Proceedings of the British Machine Vision Conference 2014.
- [16] Goodfellow, I., Pouget-Abadie, J., Mirza, M., Xu, B., Warde-Farley, D., Ozair, S., Courville, A., Bengio, Y., 2014. Generative adversarial nets. Advances in neural information processing systems 27.
- [17] Gu, A., Dao, T., 2023. Mamba: Linear-time sequence modeling with selective state spaces. arXiv preprint arXiv:2312.00752 .
- [18] Gu, A., Dao, T., Ermon, S., Rudra, A., Ré, C., 2020. Hippo: Recurrent memory with optimal polynomial projections. Advances in neural information processing systems 33, 1474–1487.
- [19] Gu, A., Goel, K., Ré, C., 2021. Efficiently modeling long sequences with structured state spaces. arXiv preprint arXiv:2111.00396 .
- [20] Guo, H., Li, J., Dai, T., Ouyang, Z., Ren, X., Xia, S.T., 2024. Mambair: A simple baseline for image restoration with state-space model, in: European conference on computer vision, Springer. pp. 222–241.
- [21] Guo, L., Huang, S., Liu, D., Cheng, H., Wen, B., 2023a. Shadow-former: Global context helps shadow removal, in: Proceedings of the AAAI Conference on Artificial Intelligence, pp. 710–718.
- [22] Guo, L., Wang, C., Yang, W., Huang, S., Wang, Y., Pfister, H., Wen, B., 2023b. Shadowdiffusion: When degradation prior meets diffusion model for shadow removal, in: Proceedings of the IEEE/CVF Conference on Computer Vision and Pattern Recognition, pp. 14049–14058.
- [23] Guo, L., Wang, C., Yang, W., Wang, Y., Wen, B., 2023c. Boundary-aware divide and conquer: A diffusion-based solution for unsupervised shadow removal, in: Proceedings of the IEEE/CVF International Conference on Computer Vision, pp. 13045–13054.
- [24] Guo, R., Dai, Q., Hoiem, D., 2012. Paired regions for shadow detection and removal. IEEE transactions on pattern analysis and machine intelligence 35, 2956–2967.
- [25] Hatamizadeh, A., Tang, Y., Nath, V., Yang, D., Myronenko, A., Landman, B., Roth, H.R., Xu, D., 2022. Unetr: Transformers for 3d medical image segmentation, in: Proceedings of the IEEE/CVF winter conference on applications of computer vision, pp. 574–584.
- [26] He, X., Cao, K., Yan, K., Li, R., Xie, C., Zhang, J., Zhou, M., 2024. Pan-mamba: Effective pan-sharpening with state space model. arXiv preprint arXiv:2402.12192 .
- [27] Ho, J., Jain, A., Abbeel, P., 2020. Denoising diffusion probabilistic models. Advances in neural information processing systems 33, 6840–6851.
- [28] Hu, V.T., Baumann, S.A., Gui, M., Grebenkova, O., Ma, P., Fischer, J., Ommer, B., 2024. Zigma: A dit-style zigzag mamba diffusion model, in: European Conference on Computer Vision, Springer. pp. 148–166.
- [29] Huang, T., Pei, X., You, S., Wang, F., Qian, C., Xu, C., 2024. Localmamba: Visual state space model with windowed selective scan, in: European Conference on Computer Vision, Springer. pp. 12–22.
- [30] Jain, J., Li, J., Chiu, M.T., Hassani, A., Orlov, N., Shi, H., 2023. Oneformer: One transformer to rule universal image segmentation, in: Proceedings of the IEEE/CVF Conference on Computer Vision and Pattern Recognition, pp. 2989–2998.
- [31] Jiang, X., Han, C., Mesgarani, N., 2025. Dual-path mamba: Short and long-term bidirectional selective structured state space models for speech separation, in: ICASSP 2025-2025 IEEE International Conference on Acoustics, Speech and Signal Processing (ICASSP), IEEE. pp. 1–5.
- [32] Jin, Y., Ye, W., Yang, W., Yuan, Y., Tan, R.T., 2024. Des3: Adaptive attention-driven self and soft shadow removal using vit similarity, in: Proceedings of the AAAI Conference on Artificial Intelligence, pp. 2634–2642.
- [33] Le, H., Samaras, D., 2019. Shadow removal via shadow image decomposition, in: Proceedings of the IEEE/CVF International Conference on Computer Vision, pp. 8578–8587.
- [34] Le, H., Samaras, D., 2021. Physics-based shadow image decomposition for shadow removal. IEEE Transactions on Pattern Analysis and Machine Intelligence 44, 9088–9101.
- [35] Li, K., Chen, G., Yang, R., Hu, X., 2024a. Spmamba: State-space model is all you need in speech separation. arXiv preprint arXiv:2404.02063 .
- [36] Li, K., Li, X., Wang, Y., He, Y., Wang, Y., Wang, L., Qiao, Y., 2024b. Videomamba: State space model for efficient video understanding. arXiv preprint arXiv:2403.06977 .
- [37] Li, S., Singh, H., Grover, A., 2024c. Mamba-nd: Selective state space modeling for multi-dimensional data, in: European Conference on Computer Vision, Springer. pp. 75–92.
- [38] Li, X., Guo, Q., Abdelfattah, R., Lin, D., Feng, W., Tsang, I., Wang, S., 2023. Leveraging inpainting for single-image shadow removal, in: Proceedings of the IEEE/CVF International Conference on Computer Vision, pp. 13055–13064.
- [39] Li, Z., Xie, G., Jiang, G., Lu, Z., 2025. Shadowmaskformer: Mask augmented patch embedding for shadow removal. IEEE Transactions on Artificial Intelligence .
- [40] Lieber, O., Lenz, B., Bata, H., Cohen, G., Osin, J., Dalmedigos, I., Safahi, E., Meirom, S., Belinkov, Y., Shalev-Shwartz, S., et al., 2024. Jamba: A hybrid transformer-mamba language model. arXiv preprint arXiv:2403.19887 .
- [41] Liu, J., Wang, Q., Fan, H., Li, W., Qu, L., Tang, Y., 2023a. A decoupled multi-task network for shadow removal. IEEE Transactions on

- Multimedia 25, 9449–9463.
- [42] Liu, Y., Guo, Q., Fu, L., Ke, Z., Xu, K., Feng, W., Tsang, I.W., Lau, R.W., 2023b. Structure-informed shadow removal networks. *IEEE Transactions on Image Processing* 32, 5823–5836.
 - [43] Liu, Y., Ke, Z., Xu, K., Liu, F., Wang, Z., Lau, R.W., 2024a. Recasting regional lighting for shadow removal, in: *Proceedings of the AAAI Conference on Artificial Intelligence*, pp. 3810–3818.
 - [44] Liu, Y., Tian, Y., Zhao, Y., Yu, H., Xie, L., Wang, Y., Ye, Q., Liu, Y., 2024b. Vmamba: Visual state space model. *ArXiv abs/2401.10166*. URL: <https://api.semanticscholar.org/CorpusID:267035250>.
 - [45] Liu, Z., Lin, Y., Cao, Y., Hu, H., Wei, Y., Zhang, Z., Lin, S., Guo, B., 2021. Swin transformer: Hierarchical vision transformer using shifted windows, in: *Proceedings of the IEEE/CVF international conference on computer vision*, pp. 10012–10022.
 - [46] Lu, Z., Li, J., Liu, H., Huang, C., Zhang, L., Zeng, T., 2022. Transformer for single image super-resolution, in: *Proceedings of the IEEE/CVF conference on computer vision and pattern recognition*, pp. 457–466.
 - [47] Mei, K., Figueroa, L., Lin, Z., Ding, Z., Cohen, S., Patel, V.M., 2024. Latent feature-guided diffusion models for shadow removal, in: *Proceedings of the IEEE/CVF Winter Conference on Applications of Computer Vision*, pp. 4313–4322.
 - [48] Niu, K., Liu, Y., Wu, E., Xing, G., 2022. A boundary-aware network for shadow removal. *IEEE Transactions on Multimedia* 25, 6782–6793.
 - [49] Qu, L., Tian, J., He, S., Tang, Y., Lau, R.W., 2017. Deshadownet: A multi-context embedding deep network for shadow removal, in: *Proceedings of the IEEE conference on computer vision and pattern recognition*, pp. 4067–4075.
 - [50] Ronneberger, O., Fischer, P., Brox, T., 2015. U-net: Convolutional networks for biomedical image segmentation, in: *Medical image computing and computer-assisted intervention–MICCAI 2015: 18th international conference, Munich, Germany, October 5–9, 2015, proceedings, part III 18*, Springer. pp. 234–241.
 - [51] Shi, Y., Xia, B., Jin, X., Wang, X., Zhao, T., Xia, X., Xiao, X., Yang, W., 2025. Vmambair: Visual state space model for image restoration. *IEEE Transactions on Circuits and Systems for Video Technology*.
 - [52] Song, Y., He, Z., Qian, H., Du, X., 2023. Vision transformers for single image dehazing. *IEEE Transactions on Image Processing* 32, 1927–1941.
 - [53] Touvron, H., Bojanowski, P., Caron, M., Cord, M., El-Nouby, A., Grave, E., Izacard, G., Joulin, A., Synnaeve, G., Verbeek, J., et al., 2022. Resmlp: Feedforward networks for image classification with data-efficient training. *IEEE transactions on pattern analysis and machine intelligence* 45, 5314–5321.
 - [54] Wan, J., Yin, H., Wu, Z., Wu, X., Liu, Y., Wang, S., 2022. Style-guided shadow removal, in: *European Conference on Computer Vision*, Springer. pp. 361–378.
 - [55] Wan, J., Yin, H., Wu, Z., Wu, X., Liu, Z., Wang, S., 2024. Crformer: A cross-region transformer for shadow removal. *Image and Vision Computing*, 105273.
 - [56] Wang, J., Gangavarapu, T., Yan, J.N., Rush, A.M., 2024. Mambabyte: Token-free selective state space model. *arXiv preprint arXiv:2401.13660*.
 - [57] Wang, J., Li, X., Yang, J., 2018. Stacked conditional generative adversarial networks for jointly learning shadow detection and shadow removal, in: *Proceedings of the IEEE conference on computer vision and pattern recognition*, pp. 1788–1797.
 - [58] Wu, H., Yang, Y., Xu, H., Wang, W., Zhou, J., Zhu, L., 2024. Rainmamba: Enhanced locality learning with state space models for video deraining, in: *Proceedings of the 32nd ACM International Conference on Multimedia*, pp. 7881–7890.
 - [59] Wu, W., Weng, J., Zhang, P., Wang, X., Yang, W., Jiang, J., 2022. Uretinex-net: Retinex-based deep unfolding network for low-light image enhancement, in: *Proceedings of the IEEE/CVF conference on computer vision and pattern recognition*, pp. 5901–5910.
 - [60] Xiao, J., Fu, X., Zhu, Y., Li, D., Huang, J., Zhu, K., Zha, Z.J., 2024. Homoformer: Homogenized transformer for image shadow removal, in: *Proceedings of the IEEE/CVF Conference on Computer Vision and Pattern Recognition*, pp. 25617–25626.
 - [61] Xu, J., Li, Z., Zheng, Y., Huang, C., Gu, R., Xu, W., Xu, G., 2025. Omnir: Shadow removal under direct and indirect lighting, in: *Proceedings of the AAAI Conference on Artificial Intelligence*, pp. 8887–8895.
 - [62] Yang, C., Chen, Z., Espinosa, M., Ericsson, L., Wang, Z., Liu, J., Crowley, E.J., 2024. Plainmamba: Improving non-hierarchical mamba in visual recognition. *arXiv preprint arXiv:2403.17695*.
 - [63] Yang, Y., Xing, Z., Yu, L., Fu, H., Huang, C., Zhu, L., 2025. Vivim: a video vision mamba for ultrasound video segmentation. *IEEE Transactions on Circuits and Systems for Video Technology*.
 - [64] Zhang, H., 2017. mixup: Beyond empirical risk minimization. *arXiv preprint arXiv:1710.09412*.
 - [65] Zhang, L., Zhang, Q., Xiao, C., 2015. Shadow remover: Image shadow removal based on illumination recovering optimization. *IEEE Transactions on Image Processing* 24, 4623–4636.
 - [66] Zhang, X., Zhao, Y., Gu, C., Lu, C., Zhu, S., 2023. Spa-former: An effective and lightweight transformer for image shadow removal, in: *2023 International Joint Conference on Neural Networks (IJCNN)*, IEEE. pp. 1–8.
 - [67] Zhao, Y., Lv, W., Xu, S., Wei, J., Wang, G., Dang, Q., Liu, Y., Chen, J., 2024. Detsr beat yolos on real-time object detection, in: *Proceedings of the IEEE/CVF Conference on Computer Vision and Pattern Recognition*, pp. 16965–16974.
 - [68] Zhu, L., Liao, B., Zhang, Q., Wang, X., Liu, W., Wang, X., 2024. Vision mamba: Efficient visual representation learning with bidirectional state space model. *arXiv preprint arXiv:2401.09417*.
 - [69] Zhu, Y., Huang, J., Fu, X., Zhao, F., Sun, Q., Zha, Z.J., 2022a. Bijective mapping network for shadow removal, in: *Proceedings of the IEEE/CVF Conference on Computer Vision and Pattern Recognition*, pp. 5627–5636.
 - [70] Zhu, Y., Xiao, Z., Fang, Y., Fu, X., Xiong, Z., Zha, Z.J., 2022b. Efficient model-driven network for shadow removal, in: *Proceedings of the AAAI conference on artificial intelligence*, pp. 3635–3643.
 - [71] Zou, Z., Yu, H., Huang, J., Zhao, F., 2024. Freqmamba: Viewing mamba from a frequency perspective for image deraining, in: *ACM Multimedia 2024*.